Advances in Motor Protection Relay Features

Ricardo Abboud, Paulo Lima, John Needs, and Alejandro Rodriguez
Schweitzer Engineering Laboratories, Inc.

Dibyendu Bhattacharya
BP Exploration Operating Co., Ltd.

ADVANCES IN MOTOR PROTECTION RELAY FEATURES

Ricardo Abboud
Schweitzer Engineering
Laboratories, Inc.
2350 NE Hopkins Court
Pullman, WA 99163
USA

Dibyendu Bhattacharya
BP Exploration Operating Co., Ltd.
Chertsey Road, Sunbury
United Kingdom

Paulo Lima
Schweitzer Engineering
Laboratories, Inc.
Avenida Pierre Simon de Laplace, 633
Condomínio Techno Park
Campinas, São Paulo 13069-320
Brazil

John Needs
Schweitzer Engineering
Laboratories, Inc.
Unit 19, Hollins Business Centre
Rowley Street, Stafford, ST16 2RH
United Kingdom

Alejandro Rodriguez
Schweitzer Engineering
Laboratories, Inc.
Hurksestraat 43, 3rd Floor
Eindhoven 5652 AH
Netherlands

Abstract—The algorithms used by numerical relays in motor thermal protection accurately simulate the characteristics of the motor. These algorithms use the motor speed to calculate rotor heat. This results in proper starting for high-inertia loads connected to motors and minimizes the cooling time, providing quicker restarts. These algorithms are performed in a numerical relay that also performs logging and plotting of starting characteristics. An accurate record of motor performance can therefore be obtained, providing an indication of possible motor failure. Broken rotor bars cause reduced accelerating torque, increased motor heating, and increased vibrations, which can inflict severe damage on a motor. Modern numerical motor relays monitor the stator current spectrum for frequency components associated with this phenomenon and use motor current signature analysis to detect broken rotor bars. For added safety, these devices can also include arc-flash protection, allowing faults in the switchgear to be quickly detected and cleared.

Index Terms—Motor protection, thermal model, arc-flash protection, broken rotor bar.

I. INTRODUCTION

Electric motor systems account for about 60 percent of global industrial electricity consumption [1]. They are fundamental to industrial processes. An undesired operation of the system protecting the motor can lead to substantial economic losses and may even compromise the safe operation of the plant.

The main function of industrial electrical power systems is to provide energy for these electric motors. Motors are subject to faults and abnormal conditions that can cause extensive damage. Motor damage can cause delays in industrial processes, with corresponding economic losses. For this reason, a reliable motor protection system is fundamental for increasing the reliability of industrial processes. This paper discusses key elements of creating a reliable motor protection system, including thermal modeling, the detection of broken rotor bars, and arc-flash detection.

Thermal protection is required to detect and protect electric motors against abnormal conditions like overload, locked rotor, frequent starts, unbalance, low-voltage operation, and others.

Installations using electromechanical relays have limited or no capabilities to accurately track motor heating conditions. In the case of large industrial motors, only numerical relays or intelligent electronic devices (IEDs) with special algorithms are able to adequately simulate actual rotor and stator thermal conditions. Modern numerical relays are the natural choice for retrofit applications, and they offer many improvements over electromechanical or static relays. These enhancements include improved thermal modeling of motor heating, event reporting, sequential event reporting, motor start reports, motor operating statistics, additional protection features (such as the detection of broken rotor bars in induction motors), and additional control functions (such as synchronous motor starting). A comprehensive thermal model that precisely represents motor heating is discussed later in this paper.

According to surveys performed by the Electric Power Research Institute (EPRI) and IEEE, 5 percent of motor failures happen because of problems in the rotor cage [2]. Early detection of a broken rotor bar is very important to minimize motor damage and reduce the time out of operation, which consequently reduces repair and operation costs. The broken-bar condition can be initiated by a fracture at the junction between the rotor bar and the end ring as the result of thermal and mechanical stressors. Motors with high-inertia loads are more susceptible to a broken rotor bar condition when starting [2]. Motor current signature analysis (MCSA) is the most popular method to detect rotor cage faults and is discussed later in the paper.

There are ten Occupational Safety and Health Administration-reportable (OSHA-reportable) arc-flash incidents every day in the United States [3]. In addition, up to 80 percent of all electrical worker injuries are due to external burns created by the intense radiant heat energy of an electrical arc flash [3].

Arc-flash detection sensors provide a cost-effective method to reduce arc-flash energy by minimizing

detection times. High-speed light detection combined with high-speed overcurrent element supervision and high-speed output contacts can provide a dependable, secure, and fast method for tripping. This, in turn, can contribute to reducing damage to equipment and significantly increasing personnel safety. Numerical motor relays can use multiple sensors for arc-flash detection. The most common sensors are lens-point sensors and bare fiber-optic sensors.

II. THERMAL MODELS

A. Motor Thermal Limits

The thermal limitations of induction motors are specified by thermal limit curves that are plots of the limiting temperatures of the rotor and stator in units of I^2t, where I is the positive-sequence, balanced stator current for a three-phase motor and t is time. The curves for a 7,000 hp, 6.6 kV, 900 rpm motor are shown in Fig. 1.
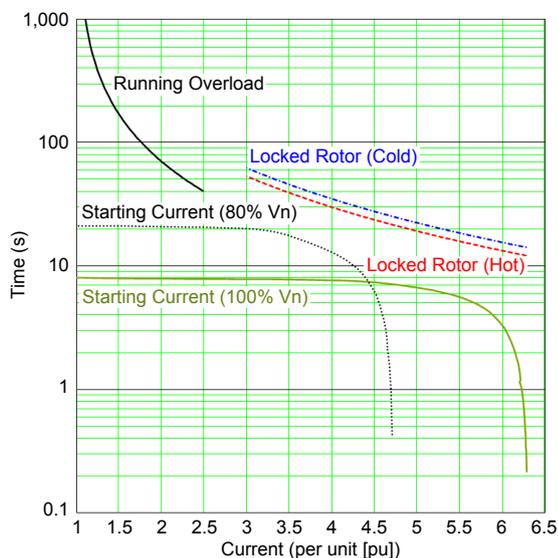
Fig. 1   Thermal limit curves for a 7,000 hp motor

The starting curves are an indication of the amount of time and associated current for the motor to accelerate from a stop condition to a full running condition. In Fig. 1 there are two starting curves: the solid curve represents the motor starting at rated voltage and the dashed curve represents the motor starting at 80 percent of the rated voltage.

Thermal protection is required to detect and protect electrical motors against abnormal conditions. Unbalances produce negative-sequence currents that can cause rotor overheating [4]. A low-voltage condition, if it occurs during normal motor operation, can cause the motor to jam. If a low-voltage condition occurs during starting, the motor may not start normally because the motor torque might be less than the load torque. In both cases, the resulting overcurrent can damage the motor. Motor stall occurs during the start operation when the motor torque cannot overpower the load torque and the motor cannot start moving.

The cause of a locked rotor may be a failure of the load bearings, a failure of the motor bearings, a low supply voltage, single phasing, or a load that exceeds

the motor torque. When the rotor is locked, the stator mimics a transformer with a resistance-loaded secondary and experiences current that is typically 6 times the rated current. Because of the rotor resistance during a locked rotor being 3 times greater than during running conditions, the effective heating due to rotor ohmic losses is 108 times that of normal operation [5].

B. First-Order Thermal Model

Motor thermal protection is responsible for removing power before a motor's temperature reaches values above of the maximum level permitted by the thermal limit curves. The actual motor heating can be calculated with a thermal model that represents the motor thermal system, as shown in Fig. 2.
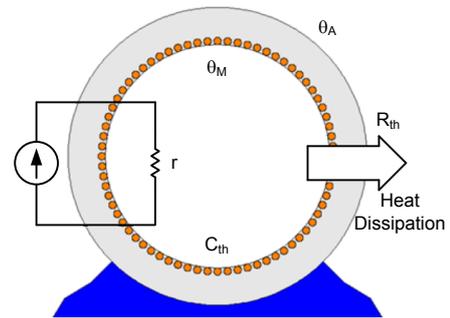
Fig. 2   Motor thermal system

The electric power applied to a motor is partially converted into heat that is stored in the motor, causing the temperature to rise. Thus, the temperature is a function of current and time. These variables are the basis of the thermal model that represents the motor temperature. A first-order thermal model is used to calculate the motor heating and is applied to the motor thermal protection [6].

Consider the motor heating caused by the current flowing through a resistor (r) that represents the resistance of the motor windings, as shown in Fig. 2. The environmental temperature is θ_A and the motor temperature is θ_M.

This simple first-order thermal system is modeled by a thermal resistance (R_{th}) to the environment and a thermal capacitance (C_{th}), with the motor considered a homogeneous body.

Fig. 3 illustrates the first-order thermal model used to represent the motor heating [5]. The major components of the model are as follows:

1. Heat source. Heat flow from the source is $I^2 \cdot r$ watts (J/s).
2. Thermal capacitance (C_{th}). This represents the capacity of the motor to absorb heat from the heat source. The unit of thermal capacitance is J/°C.
3. Thermal resistance (R_{th}). This represents the heat dissipated by a motor to its surroundings. The unit of thermal resistance is °C/W.
4. The comparator. This creates a trip condition when the calculated motor pu temperature exceeds a preset value that is based on the motor manufacturer's data, as explained in more detail later in the paper.
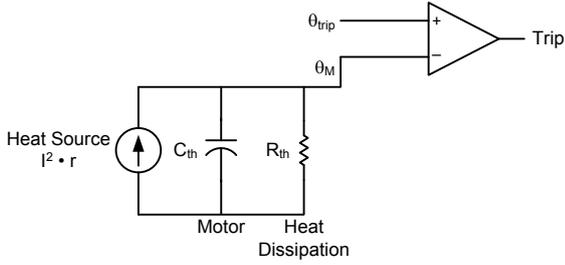
Fig. 3   First-order thermal model

Heat produced by the heat source is transferred to the motor, which in turn dissipates the heat to the surrounding environment. Motor thermal protection is implemented in modern numerical relays based on this thermal model. The relay input current is the phase motor current. The purpose of motor thermal protection is to allow the motor to start and run within the manufacturer's published guidelines and to trip if the motor heat energy exceeds those ratings due to overloads, negative-sequence current, or locked-rotor starting.

Because the positive- and negative-sequence rotor resistances (R_{r1} and R_{r2}) are functions of the motor's speed, the model becomes nonlinear. An approach used by some relay designers employs two linear models for two different stages of the motor, as shown in the Fig. 4. The limit current (I_{LIM}), which determines when each model applies, is defined by the designer. Certain relays use a limit of 2.5 times the full load current of the motor.
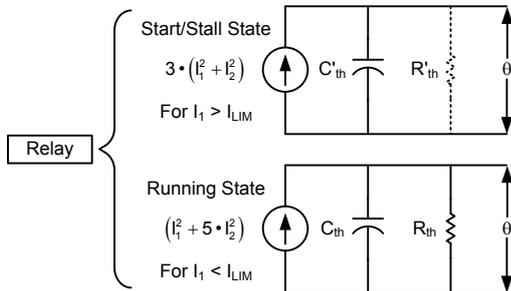
Fig. 4   Thermal models for start/stall and running states

Because locked-rotor heating occurs over just a few seconds, the start/stall state thermal model assumes that no heat is lost to the surroundings and the resistor is removed from the thermal circuit. The motor's rated locked-rotor current defines the thermal trip value.

When the motor is running, it returns heat energy to its surroundings through radiation, conduction, convection, and (in some cases) forced cooling. The running state thermal model provides a path for that energy return through the thermal resistance (R_{th}) resistor, as shown in Fig. 4.

The motor thermal characteristics (R_{th} and C_{th}) depend on many design factors. Among others, they depend on the motor size (mass). This explains why it is so difficult or impossible to emulate large motor thermal behavior with small bimetal devices. This is a clear advantage for numerical relays, in which it is possible to set different values for the motor parameters.

A slip-dependent thermal model of the rotor is discussed later in the paper.

When a motor is de-energized, it does not require thermal protection per se; however, it does need to be locked out and not allowed to re-energize until it cools down sufficiently to offer further service. When current ceases to flow in the thermal circuit shown in Fig. 3, the circuit reconfigures, as illustrated in Fig. 5, and the capacitor discharges according to the value of R_{th}.
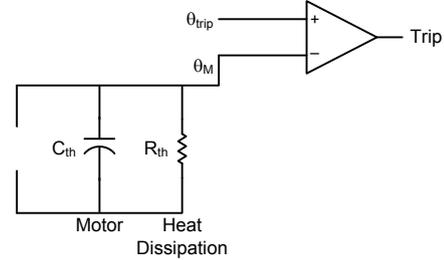
Fig. 5   Thermal model for motor stopped state

By applying the presented approach to thermal modeling, it is possible to emulate the dynamic thermal behavior of a motor, as shown in Fig. 6, to prevent damaging temperatures for any operating condition.
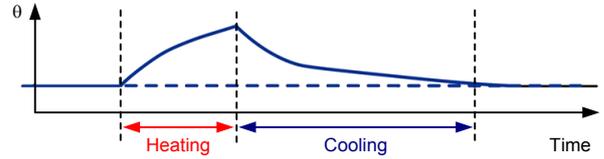
Fig. 6   Example of thermal model response for different motor states

C. Stator and Rotor Thermal Models

To accommodate the differences in stator and rotor thermal properties, the first-order thermal model can be divided into two separate thermal models, as follows:

1. The rotor model consists of the following elements:
   - A starting element that protects the rotor during the starting sequence.
   - A running element that protects the rotor when the motor is up to speed.
2. The stator model protects the stator during starting and when the motor is up to speed.

1) Rotor Model

In the rotor model, the transition from one element to the other is set at 2.5 times the rated full load current of the motor. The high-inertia starting solution using the slip-dependent thermal model described in the following subsection only affects the rotor element design.

It is valid during a starting or stalled-motor condition to neglect ambient heat losses. This results in a conservative estimate of the temperature to ensure good operation. This is equivalent to eliminating (making infinite) the thermal resistance from the model.

The rotor starting thermal limit is expressed in terms of the maximum time (motor safe stall time) that the corresponding locked-rotor current (I_{LRA}) can be applied to a motor, as calculated in (1).

$$\theta_{trip} = I_{LRA}^2 \bullet T_{STALL} \tag{1}$$

3

The rotor resistance at a speed of zero is typically 3 times that of the rotor resistance when the motor is at its rated speed. For this reason, the effect of the positive- and negative-sequence currents is multiplied by a heat source factor of 3 in the starting motor rotor thermal model.

Incorporating all of these changes results in the I^2t starting element of the first-order thermal model illustrated in Fig. 7.
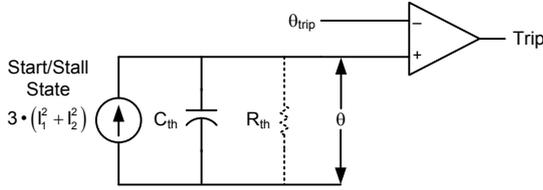
Fig. 7 I^2t starting element

To match the heat source factor of 3, the selected thermal capacitance is also 3. When the motor positive-sequence current is equal to the locked-rotor current, the estimated heat reaches the trip value within the locked-rotor time limit. Therefore, for starting protection, only the motor nameplate data are needed for the starting motor rotor thermal model.

If the temperature response of this model is plotted against the line current of the motor, the response curve is a straight line, as illustrated in Fig. 8.
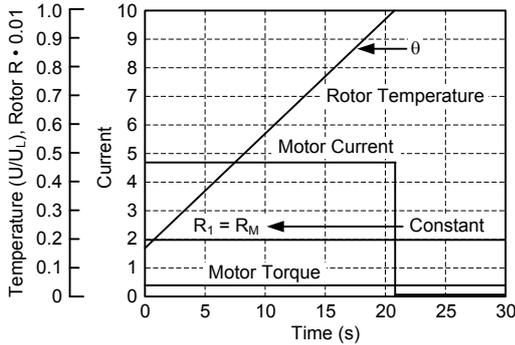
Fig. 8 I^2t starting element response curve

Note that this model keeps the rotor resistance constant at R_M, which occurs at a standstill, where the slip (S) is equal to 1.0 pu.

Fig. 9 depicts the electric analog of the first-order rotor thermal model for the motor running condition. When the motor is running, it returns heat energy to its surroundings. The running motor rotor thermal element provides a path for that energy return through the thermal resistance (R_{th}) resistor. In this state, the trip threshold "cools" exponentially from a locked-rotor threshold to the appropriate threshold for the running condition using the motor thermal time constant. This emulates a motor temperature that cools to the steady-state running condition. In the running condition, the model considers the rotor resistance to have the rated speed value ($R_r = R_N$).
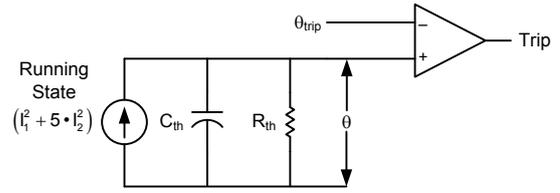
Fig. 9   Running motor rotor thermal element

2) Stator Model

The running motor overload curves show the stator thermal limit. These curves fit the time-current equation (2), where τ is the stator thermal time constant, I is the stator current in pu of rated current, I_0 is the initial current in pu of rated current, and SF is the motor service factor. This equation has the form of a first-order thermal model.

$$t = \tau \cdot \ln\left(\frac{I^2 - I_0^2}{I^2 - SF^2}\right) \qquad (2)$$

The motor stator thermal time constant is a setting parameter for the running motor thermal model, and it can be calculated from the stator thermal limit curves by applying (2).

Fig. 10 depicts the equivalent circuit that corresponds to the stator first-order thermal model. In this case, the thermal capacitance (C_{th}) equals the stator thermal time constant (τ). Assigning a value of 1 to the thermal resistance (R_{th}) resistor provides a value equal to τ for the time constant ($R_{th} \cdot C_{th}$) of the equivalent circuit. Because the positive- and negative-sequence currents have the same heating effect on the stator, the heat source equals $I_1^2 + I_2^2$. When $R_{th} = 1$, the trip threshold should equal SF^2.
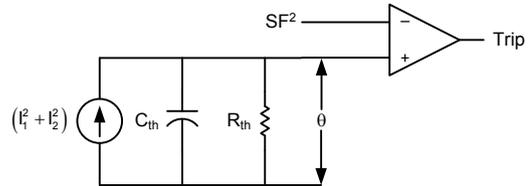
Fig. 10   Stator running thermal model

D. Slip-Dependent Thermal Model

Reference [7] derives an expression for slip-dependent rotor resistance [$R_r(S)$] in terms of the maximum rotor resistance (R_M), which occurs at a standstill (S = 1), and the normal rotor resistance (R_N), which occurs at the rated motor speed (S = rated slip). This expression is shown in (3):

$$R_r(S) = (R_M - R_N) \cdot S + R_N \qquad (3)$$

Fig. 11 shows the rotor resistance during starting.
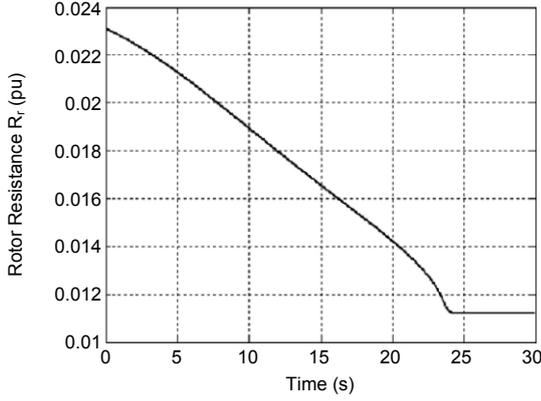
Fig. 11   Rotor resistance during starting

The values in pu of the maximum rotor resistance (R_M) and the normal rotor resistance (R_N) can be calculated by using (4) and (5) [8].

$$R_M = T_{LR} \cdot \frac{S_{LR}}{I_{LRA}^2} \tag{4}$$

where:

   T_{LR} is the locked-rotor torque in pu.

   S_{LR} is the slip when the locked-rotor condition = 1.

   I_{LRA} is the locked-rotor current in pu.

$$R_N = T_N \cdot \frac{S_N}{I_{FLA}^2} \tag{5}$$

where:

   T_N is the nominal torque in pu.

   S_N is the slip at the rated speed.

   I_{FLA} is the motor's rated current in pu.

To establish the slip-dependent thermal model, it is necessary to incorporate the slip-dependent rotor resistance into the heat source of the thermal model shown in Fig. 7.

Expressing the slip-dependent resistance value $R_r(S)$ in terms of its maximum value (R_M) and substituting it into the heat source equation provides (6):

$$W = I^2 \cdot r = I^2 \cdot \frac{R_r(S)}{R_M} \tag{6}$$

Breaking (6) down into positive-sequence (R_{r1}) and negative-sequence (R_{r2}) components accommodates motor heating caused by balanced current (positive sequence) and any current unbalance (negative sequence) that is present.

Replacing the heat source of Fig. 7 with (7) provides the slip-dependent thermal model shown in Fig. 12.

$$W_{TOTAL} = I_1^2 \cdot \frac{R_{r1}(S)}{R_M} + I_2^2 \cdot \frac{R_{r2}(S)}{R_M} \tag{7}$$
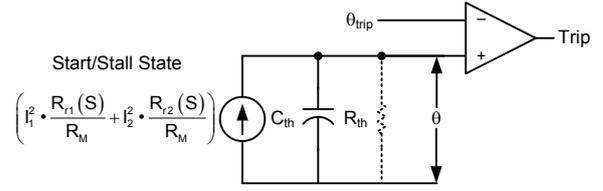
Fig. 12   Slip-dependent thermal model

E. High-Inertia Starting

In high-inertia starting, the time to accelerate a motor up to its rated speed is equal to or longer than its locked-rotor time limit. High-inertia loads, such as induced-draft fans, require long accelerating times and can exceed the allowable locked-rotor thermal limit. Prolonged starts are safely permitted in some situations because the rotor resistance $R_r(S)$ is a function of slip and decreases as the motor accelerates.

The starting current of an induction motor at the beginning of the start nearly equals the locked-rotor current magnitude but has a lesser heating effect during the start because rotor resistance decreases as the motor accelerates to rated speed.

A comparison of the conventional I^2t starting element response curve to the slip-dependent starting element response curve is shown in Fig. 13. The comparison clearly shows that, because of the decreasing rotor resistance as the motor accelerates, rotor temperature is not a linear relationship. This provides the ability to facilitate high-inertia starts without premature motor trips.
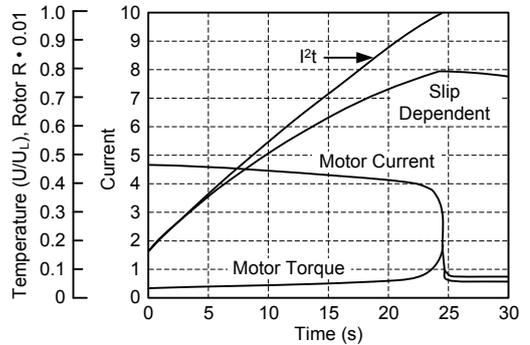
Fig. 13   Comparison of starting element response curves

III. DETECTING BROKEN ROTOR BARS

The detection of a broken rotor bar as soon as it occurs is essential to minimize damage and reduce the time and cost to repair the motor. According to [2], the broken-bar condition results from mechanical and thermal stresses that lead to a fracture at the junction between the rotor bar and the end ring.

In order to detect a broken-bar condition, MCSA can be applied [9] [10]. With this method, the frequency spectrum of the stator current is calculated and analyzed to check whether lower and upper sidebands (i.e., $[1 \pm 2S]f_0$, where f_0 is the nominal frequency) are present in the stator current, indicating that the rotor has broken bars. The magnitude of the sidebands is proportional to the number of bars that are broken.

A. Broken-Bar Detection Element

Reference [2] describes a broken-bar detection element (BBDE) with zero settings. The BBDE algorithm runs periodically to detect a broken-bar condition. It is composed of three steps: initialization, data collection, and data processing. During the initialization step, the algorithm calculates a new current from the phase currents that does not include the portion that flows to ground. It then records this current magnitude and the system frequency. A motor-running condition is detected during the data collection step using these values as a reference.

During the data collection step, the algorithm squares the current calculated in the initialization step to decouple the frequency of interest from the power system frequency and to move both sidebands into the same frequency. This squared current is also passed through a low-pass filter. Finally, the algorithm stores a collection of consecutive samples, referred to as a samples window, in digital memory.

During the data processing phase, the algorithm computes the fast Fourier transform of the samples window data and then calculates the magnitude associated with each frequency component. Finally, the average magnitudes of the frequency components are compared with a healthy motor threshold. Figure 14 in [2] shows the thresholds on the frequency spectrum of a motor running at 50 percent load with one broken bar.

B. Experimental Results

Reference [2] also presents some experimental results of the method described in this section using actual broken rotor bars. For the experimental tests, a healthy motor and motors with one, two, or three broken bars had their current frequency spectrums compared when running at 50 percent of the nominal load. The results are shown in Figure 27 in [2]. The values of the sideband peaks clearly increase as the number of broken bars increases.

Different load conditions were also experimentally tested, and the results are shown in Figure 28 in [2]. The frequency of the sideband peaks decreases as the load level decreases, and the peaks become undetectable when the motor is unloaded.

Reference [2] describes how broken bars can be erroneously detected during low-frequency source voltage oscillations. It also recommends some strategies to differentiate a broken-bar condition from a voltage oscillation (e.g., verify if all motors connected to the same feeder show the same current spectrum, and measure the voltage farther away from the motor and closer to the source to confirm the presence of low-frequency components on the power supply). In addition, these low-frequency voltage oscillations may not be present in the system all of the time. They typically appear when the system is heavily loaded or very lightly loaded.

Low-frequency load oscillations can cause current signatures similar to those of a motor with broken bars [2]. One method of differentiating the two is to apply an algorithm that detects the presence of a greater-than-normal frequency component, which may indicate a broken-bar condition.

To detect broken rotor bar conditions in different situations and monitor how they evolve, the event history and fast Fourier transform function can be applied in conjunction. This makes it possible to differentiate situations involving voltage sources with low-frequency components and oscillating loads from the broken-bar condition.

IV. ARC-FLASH DETECTION

Applying traditional time coordination for industrial systems, like motor control centers (MCCs), can lead to high fault-clearing times. Fault clearing times are typically between 0.5 and 1.0 second. However, high fault current in combination with long fault clearing times causes a very high arc-flash energy, which is a highly undesirable situation [11]. Therefore, the goal is to reduce the fault clearing time in order to reduce the arc-flash energy.

One option to reduce arc-flash energy in radial substations is to apply a simple and economical zone-interlocked blocking scheme, sometimes called a fast bus-tripping scheme. This scheme provides relatively high-speed fault clearing for buses that do not have differential protection. Instead of relying on a traditional coordination interval in the bus main relay, this scheme only requires a short delay to allow the feeder relays to block the bus main relay for a fault external to the bus. The scheme can operate for bus faults in approximately 2 to 3 cycles.

Fig. 14 shows an event report for a real fault on a 480 V bus with an arc flash. The fault started as a single-line-to-ground (SLG) fault on Phase B. After 1 cycle it evolved into a three-phase fault with a considerable increase in the fault current level. Even in impedance-grounded systems that have low current levels for SLG faults, such faults represent a high risk in terms of arc flash because of the fault evolving.

Another interesting observation about Fig. 14 is the fact that the fault current is not a pure sine wave at the fundamental frequency. This is because the arc resistance is not constant, and it plays an important role in low-voltage systems. Overcurrent relays that operate based on fundamental components calculate an incorrectly low value for the fault current, which can compromise the tripping of the instantaneous overcurrent element.

The most effective method to reduce fault clearing times is applying arc-flash protection with light sensors combined with fast overcurrent elements. Some modern numerical motor relays have incorporated arc-flash detection and support the connection of multiple sensors.
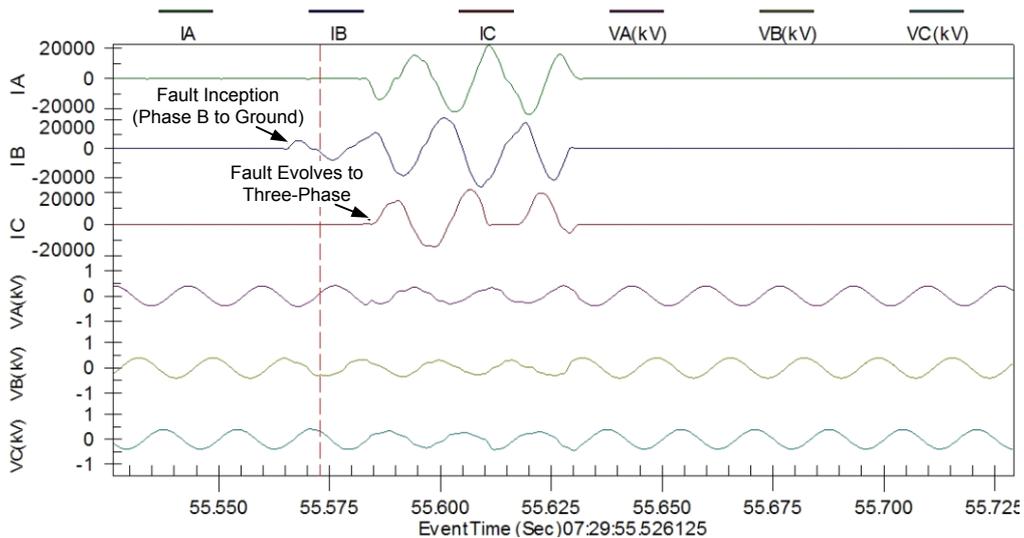
Fig. 14 An event report for a real fault on a 480 V bus with an arc flash

The purpose of detecting arc flashes is to accelerate accurate decisions to trip the circuit breaker and interrupt the fault. Arc-flash detection in a protective relay minimizes trip time, cost, and complexity. Enabling arc-flash detection in the relay makes use of the current monitoring and protection already in the circuit.

Arc-flash detection sensors provide a clear measurement of an arc flash because the light emitted during an arc-flash event is significantly brighter than the normal background substation light. It is also possible to supervise their operation with a fast overcurrent element, as discussed later in this section. The light surge is visible from the initiation of the flash and is easily detected using proven technology. The most common sensors are lens-point sensors and bare fiber-optic sensors.

The light is channeled from the sensor to the detector located in the protective relay. Monitoring the system integrity is accomplished using a fiber-optic loop. In the case of lens-point sensors (see Fig. 15), each lens has an input and an output connection. The input is connected to a transmitter in the relay, and the output is connected to a detector in the relay. This loop connection allows periodic testing of the system by injecting light from the transmitter through the loop and back to the detector. This loop connection system works with either a lens-point sensor or a bare fiber-optic sensor.

Fig. 15 Lens-point sensor

A bare fiber-optic sensor consists of a high-quality plastic fiber-optic cable without a jacket (see Fig. 16). The clear fiber-optic cable becomes a lens that captures light from the area. Using a bare fiber-optic sensor makes possible the detection of arc flashes in large areas with only one sensor.
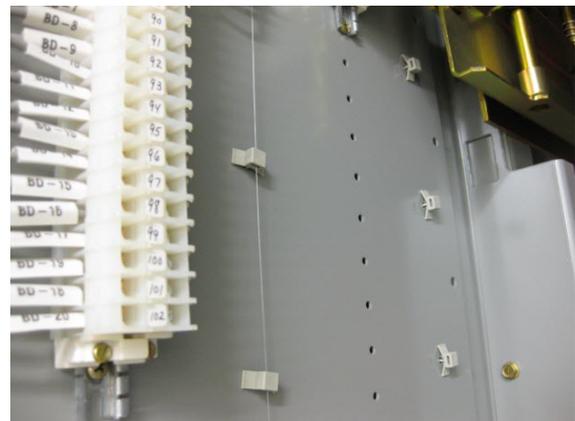
Fig. 16 Bare fiber-optic cable

Arc-flash detection systems typically use a combination of lens-point and bare fiber-optic sensors. Proper installation of the sensors and relays provides logical detection and trip points in any system.

Sensors should be located where arc-flash detection can trip the corresponding upstream circuit breaker. Using multiple sensors and having motor and feeder relays that support connections to light sensors, as shown in Fig. 17, provides 100 percent coverage for arc-flash protection that operates in the order of 2 to 3 ms.
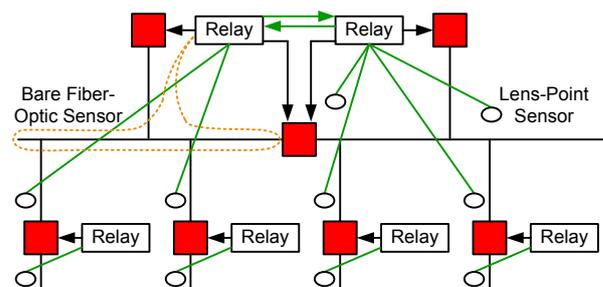
Fig. 17 Typical arc-flash detection system with sensors and relay-to-relay communication

The installation of sensors varies depending on the switchgear manufacturer, type of gear, and number of sections. Multiple sensor inputs provide coverage and sectioning options. One bare fiber-optic sensor can provide excellent coverage for an entire bus section. Lens-point sensors provide better detection in small, confined spaces.

One obstacle to using light sensors is the need to measure and adjust for changing ambient light levels. Relays store analog measurements of light and current values. Users can view these measurements and set the normal light levels for the application. Relay event reporting also provides a commissioning and troubleshooting tool with time-tagged events, including sensor light levels.

In order to add security to an arc-flash detection scheme, a high-speed overcurrent element can be applied in conjunction with the light sensors, as shown in Fig. 18, without sacrificing trip speeds. The high-speed overcurrent element is based on raw samples in order to avoid the long delays of filtering. The added advantage of processing the arc-flash detection in the protective relay is the ability to use a true overcurrent measurement as a supervising element to improve security. Setting the current level below the normally expected load enables the arc-flash detector as the trip mechanism and removes any time lag; however, it sacrifices security and makes the system dependent on light detection alone and must be avoided.
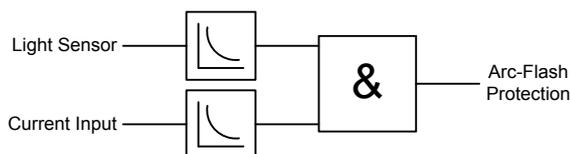
Fig. 18   Light detection in combination with high-speed overcurrent element

V.   CONCLUSIONS

Motor protection is greatly enhanced by numerical relays. Induction motors require thermal protection to prevent overheating for cyclic as well as steady-state overloads.

The heat rise in a motor caused by $I^2 \cdot r$ watts is a first-order process that can be represented by a first-order thermal model, which a motor relay can use to continuously calculate the temperature in real time. The calculated temperature is monitored to prevent overheating.

The slip-dependent thermal model tracks the motor temperature more accurately than the I^2t model, thus facilitating high-inertia starts without the use of speed switches.

BBDE algorithms that apply MCSA in modern numerical motor relays, in conjunction with the event history and the fast Fourier transform function, permit the detection of broken rotor bars under a wide variety of motor conditions. The detection element identifies the most common broken-bar cases. The event history records and makes possible more accurate analysis of when problems start and how they evolve.

Arc flashes present a clear danger to personnel. Worker safety should always be at the forefront of

designs, processes, and procedures. The addition of arc-flash detection improves the safety of installations. Arc-flash detection systems can be designed into new switchgear or retrofitted into existing gear. The security of arc-flash detection systems can be increased by parallel overcurrent and light-detection systems.

VI.   REFERENCES

[1]   T. Fleiter, W. Eichhammer, and J. Schleich, "Energy Efficiency in Electric Motor Systems: Technical Potentials and Policy Approaches for Developing Countries," United Nations Industrial Development Organization, Vienna, Austria, November 2011. Available: https://www.unido.org.

[2]   C. Pezzani, P. Donolo, G. Bossio, M. Donolo, A. Guzmán, and S. E. Zocholl, "Detecting Broken Rotor Bars With Zero-Setting Protection," proceedings of the 48th Industrial & Commercial Power Systems Technical Conference, Louisville, KY, May 2012.

[3]   T. E. Neal and R. B. Hirschmann, "The Myths and Realities of Arc Flash Protection," *Electric Energy Magazine*, May/June 2004.

[4]   P. Whatley, M. Lanier, L. Underwood, and S. Zocholl, "Enhanced Motor Protection With the Slip-Dependent Thermal Model: A Case Study," proceedings of the 34th Annual Western Protective Relay Conference, Spokane, WA, October 2007.

[5]   S. E. Zocholl, *AC Motor Protection*. Schweitzer Engineering Laboratories, Inc., Pullman, WA, 2003.

[6]   S. E. Zocholl, "Optimizing Motor Thermal Models," proceedings of the 53rd Annual Petroleum and Chemical Industry Conference, Philadelphia, PA, September 2006.

[7]   S. E. Zocholl and G. Benmouyal, "Using Thermal Limit Curves to Define Thermal Models of Induction Motors," proceedings of the 28th Annual Western Protective Relay Conference, Spokane, WA, October 2001.

[8]   S. E. Zocholl and E. O. Schweitzer, III, "Protection of Large Induction Motors – Practice vs. the Actual Model," proceedings of the 39th Annual Georgia Tech Protective Relaying Conference, Atlanta, GA, May 1985.

[9]   H. W. Penrose, *Electrical Motor Diagnostics*, 2nd ed. Success by Design, 2008.

[10] G. B. Kliman, R. A. Koegl, J. Stein, R. D. Endicott, and M. W. Madden, "Noninvasive Detection of Broken Rotor Bars in Operating Induction Motors," *IEEE Transactions on Energy Conversion*, Vol. 3, Issue 4, December 1988, pp. 873–879.

[11] J. Buff and K. Zimmerman, "Application of Existing Technologies to Reduce Arc-Flash Hazards," proceedings of the 60th Annual Conference for Protective Relay Engineers, College Station, TX, March 2007.

VII. VITAE

Ricardo Abboud received his B.S.E.E. degree in electrical engineering from Universidade Federal de Uberlândia, Brazil, in 1992. In 1993, he joined CPFL Energia as a protection engineer. In 2000, he joined Schweitzer Engineering Laboratories, Inc. (SEL) as a field application engineer in Brazil, assisting customers in substation protection and automation. In 2005, he became the field engineering manager, and in 2014, he became the engineering services manager. In 2016, he transferred to Pullman, Washington, and is currently an international technical manager. He is a certified instructor at SEL University, and has authored and coauthored several technical papers.

ricardo_abboud@selinc.com

Dibyendu Bhattacharya graduated from Jadavpur University, India, in 1991 with a bachelor of electrical engineering first-class honours degree. He worked for 14 years with the Indian Oil Corporation Ltd. refineries division, testing, commissioning, troubleshooting, and maintaining electrical equipment and power systems. He worked for the Kuwait National Petroleum Company, as well as Fluor Limited and KBR, as a lead engineer for oil and gas projects before joining BP. He has presented papers at PCIC London and coauthored one paper. He is a Chartered Engineer and a Fellow of the Institution of Engineering and Technology (IET) in the United Kingdom.

dibyendu.bhattacharya@uk.bp.com

Paulo Lima received his B.S.E.E. from Federal University of Itajubá (UNIFEI), Brazil, in 2012. He has been an application protection engineer for Schweitzer Engineering Laboratories, Inc. since 2012, providing technical support for industrial customers in Brazil.

paulo_lima@selinc.com

John Needs graduated from the University of Bath in 1981 with a degree in physics with physical electronics. He started work with GEC Measurements in 1982 as a development engineer, initially working in type testing and then programming distance relays. Next, he was a relay engineer for National Grid and later joined Alstom, first as an application engineer and then as an instructor in the training department. In 1998, Mr. Needs joined Schweitzer Engineering Laboratories, Inc., where he currently works as a regional technical manager.

john_needs@selinc.com

Alejandro Rodriguez graduated from the Universidad Metropolitana, Venezuela, in 2006 with an M.Sc. in electrical engineering. In 2006, he joined Honeywell in Caracas, Venezuela, as a junior engineer in sector automation, programming and configuration of control strategies, and human-machine interface development. In 2009, he joined Gruppo Loccioni in Angeli di Rosora, Italy, as a junior electrical engineer in electrical industrial system design and power generation systems. He joined Schweitzer Engineering Laboratories, Inc. in 2010 as a junior engineer and is currently working as an application engineer in protection in Eindhoven, Netherlands. He is a licensed professional electrical engineer.

alejandro_rodriguez@selinc.com